RSC Advances

PAPER

View Article Online
View Journal | View Issue

Cite this: *RSC Adv.*, 2020, **10**, 4545

An exclusive deposition method of silver nanoparticles on TiO_2 particles *via* low-temperature decomposition of silver-alkyldiamine complexes in aqueous media†

Tomohiro Yahagi,[ab] Takanari Togashi[a] and Masato Kurihara*[a]

An exclusive deposition method of Ag nanoparticles (NPs) on TiO_2 particles has been developed. Ag NPs supported on TiO_2 particles, Ag_x/TiO_2, with various Ag weight ratios *versus* total weights of Ag and TiO_2 between $x = 2$ and 16 wt% are prepared *via* low-temperature thermal decomposition of Ag(I)–alkyldiamine complexes generated by a reaction between $AgNO_3$ and *N*,*N*-dimethyl-1,3-propanediamine (dmpda) in an aqueous medium suspending TiO_2 particles. The thermal decomposition of the Ag(I)–alkyldiamine complexes is accelerated by TiO_2 particles in the dark, indicating that the reaction catalytically occurs on the TiO_2 surfaces. Under optimised reaction conditions, the thermal decomposition of the complex precursors is completed within 3 hours at 70 °C, and Ag NPs are almost exclusively deposited on TiO_2 particles with high conversion efficiencies (≥95%) of the precursor complexes. The thermal decomposition rates of the precursor complexes are strongly influenced by the chemical structure of a family of water-soluble dmpda analogues, and dmpda with both primary and tertiary amino groups is adopted as a suitable candidate for the exclusive deposition method. The number-averaged particle sizes of the Ag NPs are 6.4, 8.4, 11.8 and 15.2 nm in the cases of Ag_x/TiO_2, $x = 2$, 4, 8 and 16, respectively. To the best of our knowledge, the as-prepared Ag_x/TiO_2 samples show one of the highest catalytic abilities for the hydrogenation reduction of 4-nitrophenol into 4-aminophenol as a model reaction catalysed by Ag NPs.

Received 9th December 2019
Accepted 17th January 2020

DOI: 10.1039/c9ra10307d

rsc.li/rsc-advances

1. Introduction

The unique catalytic abilities of Ag metals have been utilised for industrial applications such as the production of ethylene oxides and formaldehydes.[1,2] Recently, the focus has been on Ag nanoparticles (NPs) as high performance catalysts for the hydrogenation reduction of aromatic NO_2 to NH_2 groups,[3] the reduction of carbonyl compounds,[4] the oxidation of alcohols[5] and the oxidation of CO.[6] Specifically coloured Ag NPs due to the surface plasmon resonance have elicited interest in discovering new photochemical activities.[7] Because Ag is one of the most inexpensive noble metals, the further improved catalytic activities of Ag NPs would strongly contribute to the construction of industrially available reactions for chemical syntheses and environmental purification.[8,9]

Metallic NP catalysts deposited on various supports such as oxide particles of TiO_2, Al_2O_3, and SiO_2 have been comprehensively developed.[10] These NP catalysts have been advantageously employed because of the ease of separating the support particles from the reaction media and suppressing the agglomeration of the NPs. It is well known that the catalytic activities of metal NPs are greatly affected by their sizes and morphologies, which are derived from the increased surface area by downsizing and the appearance of the specific catalytic crystal faces.[11,12] To obtain high performance catalysts, it is ordinarily necessary to increase the surface area of NPs by means of downsizing NPs and densifying NPs on supports, which also saves precious resources.

Various technologies have been developed to deposit Ag NPs on supports.[13] Conventional methods such as impregnation,[14,15] sol–gel[16,17] and colloidal[18] techniques have been employed; however, these include complicated and/or time-consuming reaction pathways and/or high-temperature treatments of more than 300 °C for the decomposition reduction of precursor silver salts.[13–18] With an eye toward environmentally friendly technologies, the invention of much simpler, lower-temperature and wasteless deposition of downsized and densified Ag NPs on supports has been indispensable.

Photo-deposition[19,20] and chemical reduction[21–24] are typical low-temperature protocols. In the photo-deposition method, Ag

[a]*Faculty of Science, Yamagata University, 1-4-12 Kojirakawa-machi, Yamagata 990-8560, Japan. E-mail: kurihara@sci.kj.yamagata-u.ac.jp*

[b]*Technical Support Center, National Institute of Technology, Tsuruoka College, 104 Sawada, Inooka, Tsuruoka, Yamagata 997-8511, Japan*

† Electronic supplementary information (ESI) available. See DOI: 10.1039/c9ra10307d

NPs are directly deposited on TiO_2 support particles from silver salts dissolved in water by photo-irradiation. The chemical reduction method has been widely utilised for the deposition of Ag NPs on support particles, where $AgNO_3$ is reduced in aqueous media by the addition of water-soluble reducing agents such as $NaBH_4$,[21] H_2O_2,[22] formaldehydes[23] and trisodium citrate.[24] However, a critical problem is the difficulty in the exclusive (wasteless) deposition of Ag NPs on support particles as well as in controlling their size, because the reduced Ag particles also unexpectedly appear and grow throughout the aqueous medium and the reaction vessel's wall. For achieving an exclusive photo-deposition method of Ag NPs on TiO_2 support particles, Ma *et al.* utilised separately prepared Ag NP seeds.[25] Dinh *et al.* succeeded in a size- and population-controllable photo-deposition method of Ag NPs on TiO_2 support particles by capping TiO_2 surfaces with hydrophobic surfactants.[26] Jiang *et al.* reported on the selective attachment of Ag NPs on the SiO_2 support particles *via* the surface functionalization of SiO_2, where the Ag NPs were generated *in situ* by the chemical reduction of Ag salts or were provided using their separately prepared seeds.[27,28] However, the conversion efficiencies of the Ag resources to Ag NPs on the support particles have not definitely been discussed.[26–28] Accordingly, the development of easily controllable reaction systems for exclusive deposition methods of Ag NPs on surface-unmodified support particles is still a challenging research subject.

Via thermal decomposition, Ag(I)–alkylamine complexes can be directly transformed into alkylamine-passivated Ag NPs whose temperatures are lower than those of the original Ag(I) inorganic salts.[29–33] In a typical case, Ag(I) oxalate, $Ag_2(C_2O_4)$, is reacted with various alkylamines to form dinuclear Ag(I)–alkylamine complexes bridged by an oxalato ligand. The decomposition temperature ranges from 100 to 150 °C, while that of the original $Ag_2(C_2O_4)$ is more than 200 °C.[29,30] The counter anion, $C_2O_4^{2-}$, functions as a reducing agent itself and is decomposed with the evolution of CO_2. If the counter anion shows a poor reducing ability in the case of $AgNO_3$, the thermal decomposition of the Ag(I)–alkylamine complexes into Ag NPs has been realised by adopting suitable structures of alkylamines as reducing agents. Kim *et al.* reported that $AgNO_3$ was decomposed between 45 and 50 °C in absolute ethanol containing butylamine for the selective deposition of Ag NPs on SiO_2 support particles by using a reaction vessel made of polyethylene to avoid the co-generation of Ag metals on glass (SiO_2) wares; nevertheless, the conversion efficiency of $AgNO_3$ to Ag NPs on SiO_2 support particles was not disclosed.[34–36] In our previous study, we reported on a low-temperature decomposition reaction of a water-soluble $Ag_2(C_2O_4)$ complex coordinated by a specific alkylamine, *N*,*N*-dimethyl-1,3-propanediamine (dmpda), catalysed by TiO_2 support particles.[37] However, the role of the alkylamine leading to the thermal decomposition has not been elucidated.

In this study, we have explored suitable reaction conditions leading to the exclusive deposition of Ag NPs on TiO_2 support particles *via* the thermal decomposition of Ag(I)–alkyldiamine complexes derived from a general Ag(I) resource, $AgNO_3$. It is revealed that Ag(I)–alkyldiamine complexes are catalytically decomposed and deposited on the TiO_2 particle surfaces in an environmentally friendly solvent, water, at moderate temperatures, and the conversion efficiencies of the precursor complexes into Ag NPs exceed 95% by adjusting a crucial reaction factors of the chemical structures of alkyldiamines, the decomposition temperatures and the decomposition times. The number-averaged particle sizes of the Ag NPs are controlled by the concentrations of Ag(I)–alkyldiamine complexes. To the best of our knowledge, the as-prepared Ag NPs on TiO_2 support particles show one of the highest catalytic abilities *via* hydrogenation reduction from 4-nitrophenol to 4-aminophenol using $NaBH_4$ as a model reaction catalysed by Ag NPs.

2. Experimental

2.1 Materials

$AgNO_3$ (99.7%) and anatase-type TiO_2 (>99.0%) particles (50–300 nm) were purchased from Kanto Chemicals and Merck, respectively. *N*,*N*′-Dimethyl-1,3-propanediamine (>97%) was purchased from Aldrich. Propylamine (>98%), 1,3-propanediamine (>98%), *N*-methyl-1,3-propanediamine (>98%), *N*,*N*-dimethyl-1,3-propanediamine (dmpda) (>99%) and *N*,*N*,*N*′,*N*′-tetramethyl-1,3-propanediamine (>98%) were obtained from Tokyo Chemical Industry. Nitric acid (60–61%), deuterium oxide (>99.9%), $NaBH_4$ (>95%) and 4-nitrophenol (>99%) were supplied by Wako Pure Chemical Industries Ltd. All chemicals were used without further purification.

2.2 Methods

In a typical method for preparing the Ag nanoparticles (NPs) supported on TiO_2 particles (Ag_x/TiO_2) with various Ag weight ratios *versus* total weights of Ag and TiO_2 between $x = 2$ and 16 wt%, aqueous solutions of Ag(I)–alkyldiamine (–dmpda) complexes were prepared by adding various volumes (378 μL ($x = 2$), 772 μL (4), 1.61 mL (8) and 3.53 mL (16)) of an $AgNO_3$ solution (1.00 mol L^{-1}) into an ice-cooled mixture of water (10 mL) and dmpda with vigorous stirring, where the molar ratio of dmpda to $AgNO_3$ was fixed at 4. An aqueous suspension (90 mL) of TiO_2 particles (2.00 g) was controlled at various constant temperatures under a nitrogen atmosphere. The aqueous solution of the Ag(I)–dmpda complexes was added into the aqueous suspension of TiO_2 particles with vigorous stirring. The thermal decomposition reaction of the Ag(I)–dmpda complexes was carried out at a constant temperature in the dark. After the reaction was completed, Ag_x/TiO_2 samples were obtained by centrifugal separation and washing with water four times and then vacuum drying at room temperature.

2.3 Evaluation of the catalytic abilities of Ag_x/TiO_2

The catalytic activities of Ag_x/TiO_2 were evaluated by a typical model reaction catalysed by Ag NPs, *i.e.* a reduction reaction of 4-nitrophenol to 4-aminophenol using $NaBH_4$. A mixture of aqueous suspension (3.2 mL) of Ag_x/TiO_2 (0.020 mg) and an aqueous solution of 4-nitrophenol (0.40 mL, 6.0×10^{-4} mol L^{-1}) was placed in an optical quartz cell. A freshly prepared aqueous solution of $NaBH_4$ (0.40 mL, 0.30 mol L^{-1})

was mixed quickly to initiate the catalytic reaction. Time-course changes in the UV-Vis absorption spectra were measured at 5 second intervals at a constant temperature of 25 °C using a photodiode array spectrometer (Agilent 8453) to pursue the decreasing absorption band of 4-nitrophenol.

2.4 Characterisation

The morphologies and sizes of Ag NPs of Ag_x/TiO_2 were characterised *via* transmission electron microscope (TEM) images (JEOL JEM 2100) operating at 200 kV. All specimens for TEM were prepared by dropping a diluted suspension of Ag_x/TiO_2 on a collodion membrane-coated Cu grid. The number-averaged particle sizes, d_{av}, were calculated by measuring the long-axis lengths of more than 100 particles. The powder X-ray diffraction (XRD) patterns were obtained on an X-ray diffractometer (Rigaku MiniFlex II) equipped with a Cu Kα X-ray source (30 kV, 15 mA). ^{109}Ag nuclear magnetic resonance (NMR) spectra of the Ag(I)–alkyldiamine complexes in aqueous solutions were measured with an NMR spectrometer (JEOL ECX-400), where an aqueous solution of $AgNO_3$ was used as a reference for calibrating chemical shifts (δ). The concentrations of Ag ions in aqueous media and the Ag contents of Ag_x/TiO_2 were determined by inductively coupled plasma-atomic emission spectroscopy (ICP-AES, SII Nanotechnology, SPS 3500-DD). X-ray photoelectron spectroscopy (XPS) was carried out using a Shimadzu ESCA-3200 photoelectron spectrometer equipped with a Mg Kα X-ray source ($h\nu$ = 1253.6 eV, 10 kV, 30 mA). The binding energy of the Ag NPs of Ag_x/TiO_2 was calibrated by setting the C 1s peak to 284.8 eV.

3. Results and discussion

3.1 Exclusive deposition of Ag NPs on TiO_2 particles

Ag NPs supported on TiO_2 particles, Ag_x/TiO_2, with various Ag weight ratios *versus* total weights of Ag and TiO_2 between x = 2, 4, 8 and 16 wt% were prepared *via* low-temperature thermal decomposition of Ag(I)–alkyldiamine (–dmpda) complexes. The concentration of Ag components dissolving in aqueous media decreased and almost disappeared within 3 hours by low-temperature heating at 70 °C (Fig. 1). In the absence of TiO_2 particles, the rate of decrease of Ag components was significantly suppressed, *vide infra* (Fig. 6a, red line), and the TiO_2 particles initially exhibited purple in colour along with decreasing concentrations of Ag components. The colour originated from the surface plasmon resonance of metallic Ag NPs. These results suggest that the Ag(I)–dmpda complexes are catalytically decomposed on the TiO_2 particles in aqueous media to immobilise on their surfaces as Ag NPs.

In the XRD pattern of the pristine TiO_2 particles, the signals appearing at 25.3, 36.9, 37.8, 38.5, 48.0, 53.9, 55.1, 62.1, 62.7, 68.8, 70.3, 75.0 and 76.1° were derived from the anatase type (PDF: 01-070-7348); these signals were consistent with the (101), (103), (004), (112), (200), (105), (211), (213), (204), (116), (220), (215) and (301) faces, respectively (Fig. 2). Although the XRD-signal profile was not changed after the low-temperature thermal decomposition of Ag(I)–dmpda complexes, new weak

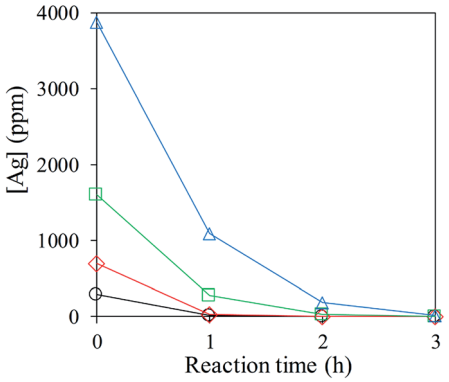

Fig. 1 Time-course changes in concentrations of Ag components dissolving in the reaction aqueous media at 70 °C in the presence of suspended TiO_2 particles. Added volumes of an $AgNO_3$ solution (1.00 mol L^{-1}) were 378 μL (○), 772 μL (◇), 1.61 mL (□) and 3.53 mL (△). The decomposition reactions were investigated in the dark.

XRD signals appeared at 38.1, 44.1, 64.5 and 77.3° in the cases of Ag_8/TiO_2 and Ag_{16}/TiO_2. These signals are assigned to the (111), (200), (220) and (311) faces of the face-centred cubic phase of metallic Ag (PDF: 01-071-3762). The signals are significantly broadened, indicating that metallic Ag is deposited as NPs on TiO_2 surfaces. Similar XRD signals due to metallic Ag cannot be clearly observed in the cases of Ag_2/TiO_2 and Ag_4/TiO_2, due to the signal broadening and low concentration of the deposited metallic Ag on TiO_2 surfaces. These results suggest that Ag(I) ions are successfully reduced to Ag(0) *via* the low-temperature thermal decomposition of Ag(I)–dmpda complexes occurring catalytically on the TiO_2 surfaces in the dark.

The morphology and sizes of Ag NPs of Ag_x/TiO_2 were investigated *via* TEM images (Fig. 3). Innumerable NPs (Fig. 3b–e) were observed as dark contrasts on the surfaces of TiO_2

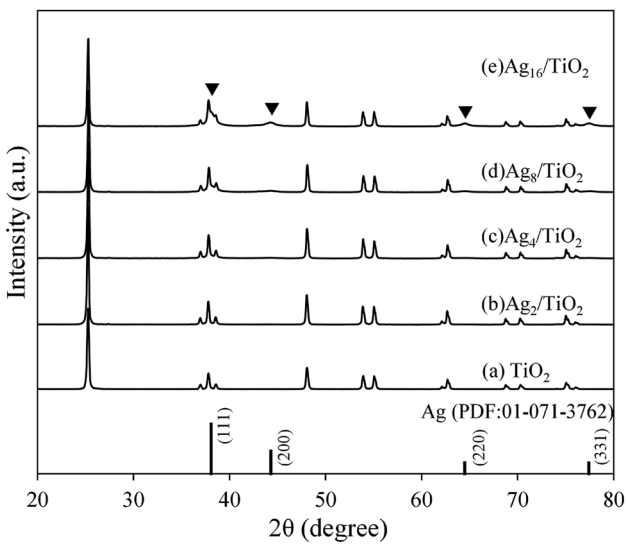

Fig. 2 XRD patterns of the pristine TiO_2 particles (a) and the Ag NP-deposited Ag_x/TiO_2, x = 2 (b), 4 (c), 8 (d) and 16 (e). The XRD signal positions due to metallic Ag are marked by ▼.

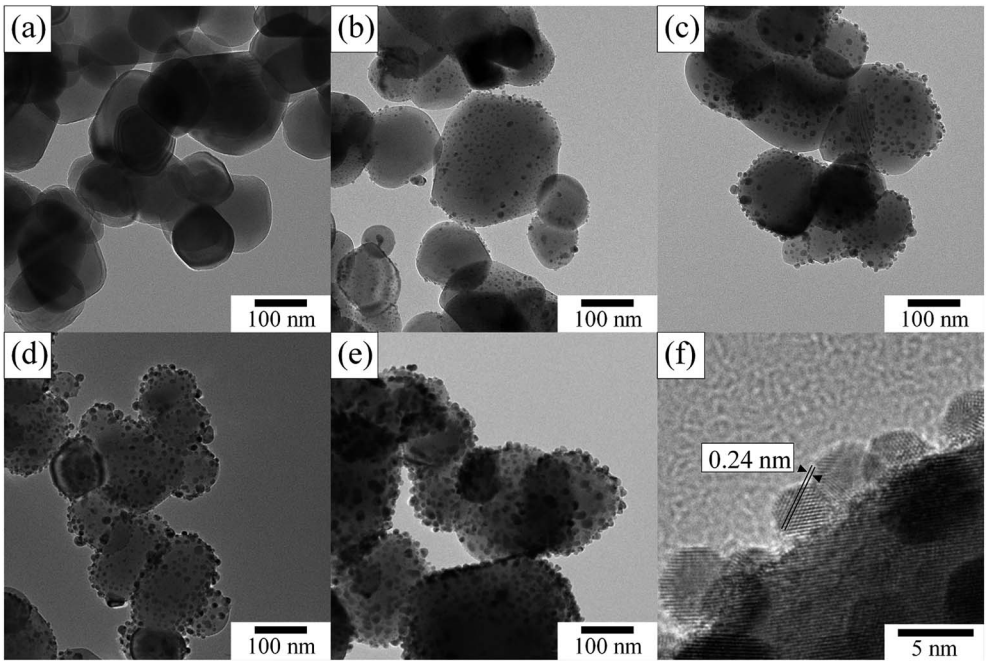

Fig. 3 TEM images of the pristine TiO_2 particles (a) and the Ag NP-deposited Ag_x/TiO_2, $x = 2$ (b), 4 (c), 8 (d) and 16 (e), and a magnified high-resolution lattice image of Ag NPs in the case of Ag_2/TiO_2 (f).

particles (Fig. 3a) between 50 and 300 nm in dimension. From high-resolution TEM images of the deposited NPs (Fig. 3f), lattice fringes can be clearly observed with lattice spacing of 0.24 nm which is consistent with (111) faces of the face-centred cubic metallic Ag.

The deposited amounts of Ag on TiO_2 particles of Ag_x/TiO_2 were determined *via* an ICP-AES technique using aqueous solutions of Ag NPs oxidatively dissolved by HNO_3. When the initial Ag contents were adopted as Ag(I)–dmpda complexes as a precursor for preparing Ag_x/TiO_2, $x = 2$, 4, 8 and 16 wt%, the actual amounts of the deposited Ag NPs on TiO_2 particles were 1.9, 3.9, 7.9 and 15.5 wt%, respectively. It is noted that the Ag(I)–dmpda complex precursors are almost exclusively deposited on TiO_2 particles through the catalytic low-temperature decomposition of the precursors on the TiO_2 surfaces with high conversion efficiencies of 95, 98, 99 and 97% in the cases of $x = 2$, 4, 8 and 16, respectively. The number-averaged particle sizes, d_{av}, of Ag NPs on the TiO_2 surfaces were calculated based on more than 100 particles from each prepared sample of Ag_x/TiO_2 (Fig. 3). The total number-averaged particle size, $d_{av,total}$, and the standard deviation, σ, were estimated from several d_{av} with sample dependency. Fig. 4 shows the plot of $d_{av,total}$ of Ag_x/TiO_2 *versus* the initial Ag contents of the Ag(I)–dmpda complex precursors, $x = 2$, 4, 8 and 16 wt%. The $d_{av,total}$ were 6.4, 8.4, 11.8 and 15.2 nm in the cases of $x = 2$, 4, 8 and 16, respectively. The particle size distributions of the deposited Ag NPs from the representative samples of Ag_x/TiO_2 are shown as histograms in Fig. 5. The size distribution of the Ag NPs becomes wider with increasing x. At this stage, the dimension of the Ag NPs is still uncontrollable in the case of $x = 16$, because the distribution is largely deviated from d_{av}.

3.2 Investigation of the optimised reaction conditions for the exclusive deposition

As the decreasing rate of the Ag components was already shown in Fig. 1, the decreasing rates, *i.e.* the thermal decomposition rates of the Ag(I)–dmpda complexes dissolving in an aqueous medium, were investigated depending on the reaction temperatures between 0 and 100 °C in the dark (Fig. 6). In the absence of TiO_2 particles (Fig. 6a), almost no consumption (no thermal decomposition) of the Ag(I)–dmpda complexes was observed at less than 60 °C within 3 hours, while the Ag(I)–dmpda complexes were suddenly consumed at elevated temperatures of ≥70 °C and disappeared from the aqueous medium within 1 hour at 100 °C. It is obvious that the presence of TiO_2 particles

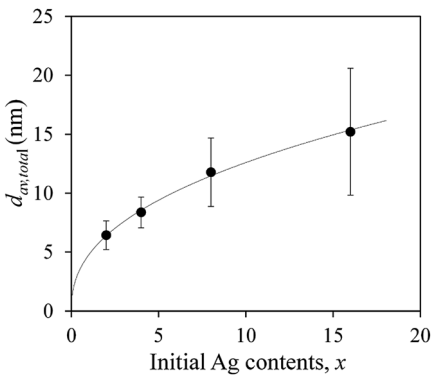

Fig. 4 Plots of total number-averaged particle sizes, $d_{av,total}$, of Ag_x/TiO_2 *versus* the initial Ag contents of the Ag(I)–dmpda complex precursors, $x = 2$, 4, 8 and 16 wt%. The error bars show the standard deviation, $\pm\sigma$.

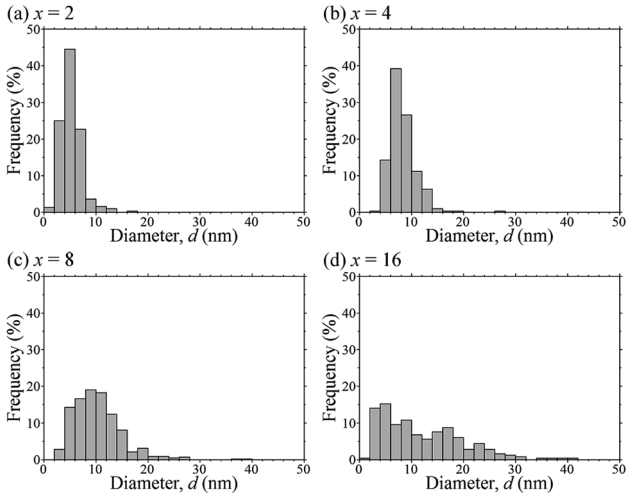

Fig. 5 The particle size distributions of the deposited Ag NPs from the representative samples of Ag_x/TiO_2, $x = 2$ (a), 4 (b), 8 (c) and 16 (d).

accelerates the thermal decomposition rate of the Ag(I)–dmpda complexes, as compared with the elevated temperatures of ≥60 °C (Fig. 6b). Consequently, we adopted 70 °C as one reaction temperature suitable for completing the exclusive deposition of Ag NPs on TiO_2 particles within a few hours.

Intriguingly, the realisation of the exclusive deposition reaction of Ag NPs on TiO_2 particles was strongly influenced by both the addition amounts and the chemical structures of water-soluble alkyldiamines (Table 1). The photographs of aqueous solutions of $AgNO_3$ in the presence of different molar ratios of dmpda are shown in Fig. S1.† The aqueous solutions were immediately clouded by black particles when an aqueous solution of $AgNO_3$ was added to an aqueous solution of dmpda with molar ratios of dmpda to $AgNO_3$ of 1.0 and 1.5 mol mol^{-1} (Fig. S1(i) and (ii)†). The XRD pattern of the black precipitates isolated from the aqueous solutions was derived from Ag_2O crystals. In the case of molar ratios of ≥2.0, colourless transparent solutions were obtained (Fig. S1(iii)–(v)†). In a ^{109}Ag-NMR spectrum of the transparent and colourless aqueous mixture of $AgNO_3$ and dmpda with a molar ratio of 1 : 4 mol mol^{-1}, one single signal was observed at 362 ppm (Fig. S2a†), when one signal of an aqueous solution of $AgNO_3$ without alkyldiamines was employed as a standard one of 0 ppm for evaluating chemical shifts. In case of Ag : dmpda = 1 : 2 mol mol^{-1}, the ^{109}Ag-NMR signal appeared at 348 ppm. This result suggests that dmpda ligands are dynamically exchanged on Ag^+ *via* the weak coordination of H_2O as a solvent molecule, depending on the concentrations of dmpda. The ^{109}Ag-NMR chemical-shift value was consistent with 363 ppm of Ag^+ coordinated by propylamine with a primary amino group in the case of Ag : propylamine = 1 : 4 (Fig. S2b†). As a result, it is generally understood that (i) Ag^+ ions can be coordinated by dmpda as a monodentate ligand to form $[Ag(dmpda)_2]^+$ *via* dynamical ligand-exchange with H_2O for dissolving in water, (ii) Ag^+ ions are coordinated by dmpda *via* the primary amino group, but not the bulky tertiary amino group, and (iii) an insoluble Ag_2O precipitate is generated by the basic aqueous conditions without stoichiometrically sufficient dmpda ligands of Ag : dmpda = 1 : 2 mol mol^{-1}.

A family of dmpda analogues was investigated to choose water-soluble alkyldiamines suitable for low-temperature thermal decomposition on TiO_2 particles, as listed in Table 1. Transparent and colourless solutions were similarly obtained by the reaction of $AgNO_3$ with 1,3-propanediamine or *N*-methyl-1,3-propanediamine, indicating that water-soluble Ag(I)–alkyldiamine complexes were stably formed by the coordination bonding of the primary amino group, whereas *N*,*N*′-dimethyl-1,3-propanediamine and *N*,*N*,*N*′,*N*′-tetramethyl-1,3-propanediamine without primary amino groups produced black particles of Ag_2O. The thermal decomposition behaviour of Ag(I)–alkyldiamine complexes composed of 1,3-propanediamine and *N*-methyl-1,3-propanediamine was compared to that of the Ag(I)–dmpda complexes. The Ag(I)–(1,3-propanediamine) complexes were scarcely decomposed at 70 °C even after 3

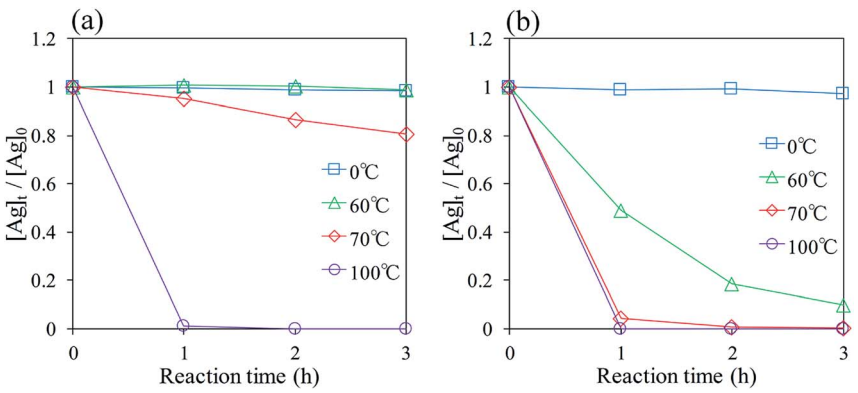

Fig. 6 Time-course changes in consumption rates of Ag components dissolving in the reaction aqueous media at various temperatures of 0, 60, 70 and 100 °C in the absence (a) or in the presence (b) of suspended TiO_2 particles. The added volume of an $AgNO_3$ solution (1.00 mol L^{-1}) was 772 μL. The consumption rates were expressed as $[Ag]_t/[Ag]_0$, where $[Ag]_0$ and $[Ag]_t$ are the initial concentration of the Ag components in the reaction media at time = 0 and the concentrations of the Ag components at various reaction times = *t*, respectively. The decomposition reactions were investigated in the dark.

Table 1 Chemical structures of the dmpda (alkyldiamine) analogues and their reaction behaviour

Alkyldiamines	Formation of Ag(I)–alkyldiamine complexes[a]	Thermal decomposition rates[b] (%)
 1,3-propanediamine	○	7%
 N-methyl-1,3-propanediamine	○	31%
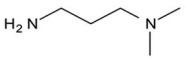 N,N-dimethyl-1,3-propanediamine (dmpda)	○	100%
 N,N′-dimethyl-1,3-propanediamine	×	N.A.
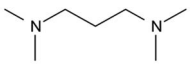 N,N,N′,N′-tetramethyl-1,3-propanediamine	×	N.A.

[a] The alkyldiamine (3.09 mmol) was dissolved in water (10 mL), and an $AgNO_3$ aqueous solution (1.00 mol L^{-1}, 772 μL) was dropwise added to the alkyldiamine solution with vigorous stirring under ice cooling, where the molar ratio is Ag : alkyldiamine = 1 : 4 mol mol^{-1}. [b] The thermal decomposition rates (%) of Ag(I)–alkyldiamine complexes for 3 h at 70 °C under the same reaction conditions and analyses as Fig. 6b.

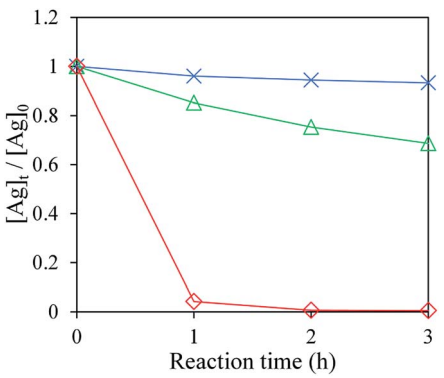

Fig. 7 Time-course changes in consumption rates of Ag components dissolving in the reaction aqueous media at 70 °C in the presence of TiO_2 using 1,3-propanediamine (×), *N*-methyl-1,3-propanediamine (△) and dmpda (◇). The aqueous solutions of Ag(I)–alkyldiamine complexes were prepared by the addition of an aqueous solution (772 μL) of $AgNO_3$ (1.00 mol L^{-1}) into to a mixture of the alkyldiamines and water (10 mL), where the molar ratio of the $AgNO_3$ and alkyldiamines is 1 : 4 mol mol^{-1}. The time-course changes in consumption rates of the Ag components were monitored after the addition of the aqueous solutions of Ag(I)–alkyldiamine complexes into an aqueous suspension (90 mL) of TiO_2 particles (2.00 g) at a constant temperature of 70 °C. The decomposition reactions were investigated in the dark.

hours, and a moderate decomposition reaction was observed in the case of the Ag(I)–(*N*-methyl-1,3-propanediamine) complexes which reached 31% decomposition after 3 hours (Fig. 7, Table 1). It is evident that stable coordination to Ag^+ ions occurs *via* the primary amino groups, and low-temperature decomposition is promoted in the order of tertiary > secondary > primary amino groups of the distal position. This order is consistent with the reduction abilities of alkylamino groups due to increased electron density on the nitrogen atom. On the basis of these results, we adopted dmpda as a suitable water-soluble alkyldiamine to realise the exclusive deposition of Ag NPs on TiO_2 particles from aqueous solutions of Ag(I)–alkyldiamine complexes.

3.3 Evaluation of the catalytic abilities of Ag_x/TiO_2

The catalytic abilities of Ag_x/TiO_2 were evaluated *via* a typical model reaction catalysed by Ag NPs, *i.e.* hydrogenation reduction of 4-nitrophenol to 4-aminophenol using $NaBH_4$.[38] In a typical time-course change in the UV-Vis absorption spectra in the case of Ag_2/TiO_2 (Fig. 8), the absorption band of 4-nitrophenol at 400 nm gradually decreased in intensity after the addition of $NaBH_4$, and completely disappeared within 6 minutes. A new absorption band originating from 4-aminophenol appeared at 300 nm with isosbestic points at 282 and 314 nm. The hydrogenation reduction of 4-nitrophenol to 4-aminophenol was catalysed by the Ag NPs deposited on TiO_2 particles because a similar spectral change was not observed in the case of pristine TiO_2 particles. Similar absorption spectral changes were also observed in the cases of $x = 4$, 8 and 16 of Ag_x/TiO_2, and the catalytic reaction of 4-nitrophenol was accelerated by increasing amounts, x of the Ag NPs, as shown in the time-course changes in the absorbance at 400 nm (Fig. 9a). In the initial stage, induction periods were observed where the absorbance did not change. The induction periods became longer as the deposited amounts of the Ag NPs were decreased. It has been explained that the induction period is caused by the reconstitution of catalyst surfaces, *i.e.* removal of oxygenated

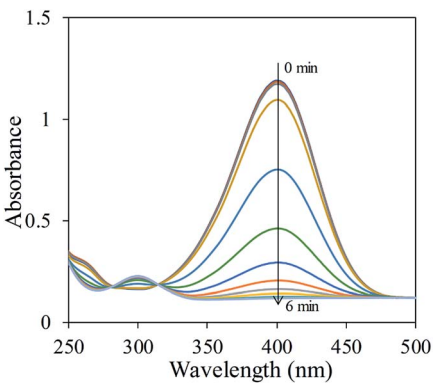

Fig. 8 UV-Vis absorption spectral change of an aqueous solution of 4-nitrophenol in 30 second intervals after the addition of $NaBH_4$ in the presence of Ag_2/TiO_2 at a constant temperature of 25 °C, where initial concentrations of 4-nitrophenol, $NaBH_4$, Ag_2/TiO_2 are 6.0×10^{-5}, 3.0×10^{-2} and 5.0 mg L^{-1}, respectively.

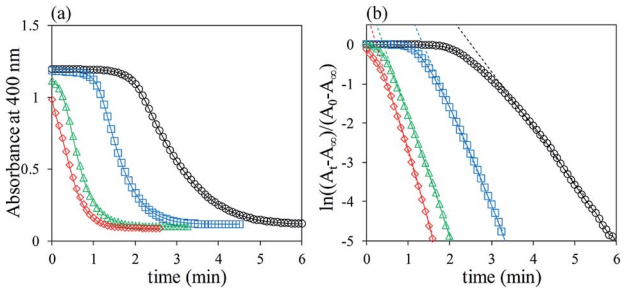

Fig. 9 (a) Time-course changes in absorbance at 400 nm and (b) their transformed plots by eqn (1) in the cases of Ag_x/TiO_2, $x = 2$ (○), 4 (□), 8 (△) and 16 (◇). The concentrations of Ag_x/TiO_2 per volumes (L) of the reaction media were prepared as 5.0 mg L^{-1} (see Table 2).

components on the surfaces of Ag NPs and/or the consumption of dissolved oxygen.[39,40] In order to evaluate the catalytic activities dependent on the deposited amounts of Ag NPs, the apparent rate constants, k, were calculated. When the largely excess amount of $NaBH_4$ to 4-nitrophenol was used in concentration, the concentration of $NaBH_4$ was assumed to be constant during the catalytic reaction. Thus, the catalytic reaction can be treated as pseudo-first-order kinetic behaviour,[38] and the apparent rate constants, k, can be expressed by the absorbance (A) at a certain reaction time (t) using the following eqn (1):

$$\ln\frac{A_t - A_\infty}{A_0 - A_\infty} = -kt \quad (1)$$

The time-course changes in absorbance (Fig. 9a) were transformed by eqn (1) (Fig. 9b). The reaction rate constants of k of Ag_x/TiO_2 were calculated by the linear approximation of plots excluding the induction periods, and were 2.3×10^{-2}, 4.0×10^{-2}, 4.7×10^{-2} and 5.8×10^{-2} s^{-1} in the cases of $x = 2$, 4, 8 and 16, respectively. In order to compare the catalytic abilities of Ag_x/TiO_2 to those of the previously reported Ag catalysts, we used the normalised values, k/[Ag].[41,42] As summarised in Table 2, the concentration of catalysts, [cat.], was expressed by the weight (mg) of the catalyst per volume (L) of the reaction medium, and the concentration, [Ag], was of the actual Ag weight (g) contained in each catalyst per volume (L) of the reaction medium. The k/[Ag] values of Ag_x/TiO_2 were 240, 210, 120 and 75 s^{-1} g^{-1} L in the cases of $x = 2$, 4, 8 and 16, respectively. The catalytic abilities are improved as $d_{av,total}$ are decreased, *i.e.* as the surface areas of the Ag NPs are increased. The size-dependent nature of the catalytic abilities of the Ag NPs is also understandable *via* the turnover numbers (TONs). The catalytic abilities of Ag_x/TiO_2 are much higher than those of the previously reported Ag catalysts, on the basis of the k/[Ag]. To the best of our knowledge, Ag_x/TiO_2 samples show one of the highest catalytic abilities for a model reaction, hydrogenation reduction of 4-nitrophenol to 4-aminophenol. There is a tendency for Ag NPs on metal-oxide substrates, especially on TiO_2, to present relatively higher catalytic activities. As shown in Fig. 3f, the Ag NPs connect with the TiO_2 surfaces in hemisphere shapes, suggesting formation of strong junctions between Ag NPs and TiO_2 particles. In fact, XPS analysis showed that the binding energy (367.6 eV) of Ag NPs on TiO_2 particles was shifted to a lower energy than that of the intrinsic Ag metal (368.2 eV) (Fig. S3†). The specific electronic interaction between Ag NPs and TiO_2 particles would be responsible for the enhanced catalytic abilities of Ag_x/TiO_2. In addition, the particle

Table 2 Comparison of the catalytic abilities of Ag catalysts supported by various substrates based on the model reaction from 4-nitrophenol to 4-aminophenol

Catalysts	d^a (nm)	Ag contents in catalysts (wt%)	Concentrations of catalysts, [cat.]^b (mg L^{-1})	Rate constants (reaction temperature), k (10^{-3} s^{-1})	Catalytic abilities based on Ag, k/[Ag]^c (s^{-1} g^{-1} L)	TONs^d	Ref.
Ag_2/TiO_2	6.4	1.9	5.0	23 (25 °C)	2.4×10^2	68	This work
Ag_4/TiO_2	8.4	3.9	5.0	40 (25 °C)	2.1×10^2	33	This work
Ag_8/TiO_2	11.8	7.9	5.0	47 (25 °C)	1.2×10^2	16	This work
Ag_{16}/TiO_2	15.2	15.5	5.0	58 (25 °C)	75	8	This work
Ag NPs (no support)	14.3	100	482	0.47 (R.T.)	9.8×10^{-4}		43
Ag/porous carbon	10	55.2	333	1.7 (R.T.)	9.2×10^{-3}		44
Graphene oxide/ Ag NPs-Fe_3O_4	9–20	24.3	33.3	27 (R.T.)	3.3		45
Ag/micron-SiO_2 sphere	10–60	43.0	250	3.6 (22 °C)	3.3×10^{-2}		46
Fe_3O_4@SiO_2–Ag	3.7	8.89	16.7	7.7 (25 °C)	5.2		47
Ag/fibrous nano-silica	4	8.97	66.2	10 (20 °C)	1.7		48
TiO_2@Ag	10	9.28	13.0	7.5 (25 °C)	6.2		25
Ag/TiO_2	<1	0.75	16.0	20 (25 °C)	1.7×10^2		49

[a] Averaged particle sizes or size ranges of Ag NPs. [b] The catalyst weights (mg) per volume (L) of a reaction medium. [c] The rate constants, k, are normalized by the concentration of the actual Ag weights (g) contained in each catalyst per volume (L) of the reaction medium, [Ag]. [d] TONs are expressed by the number ratios of the initial substrate molecule (4-nitrophenol) *versus* the Ag atoms, when 4-nitrophenol is completely converted into 4-aminophenol for 360, 200, 125 and 100 seconds in the cases of Ag_x/TiO_2, $x = 2$, 4, 8 and 16, respectively (see Fig. 9).

sizes, morphologies, and distribution of the Ag NPs on TiO_2 particles were not so significantly changed after the catalytic reactions from the TEM images of the Ag_x/TiO_2 (Fig. S4†).

4. Conclusion

In this study, we focus on developing an exclusive deposition method of Ag NPs on metal oxide particles through a low-temperature decomposition reaction of water-soluble Ag(I)–alkyldiamine complexes catalysed by TiO_2 in aqueous media. It is revealed that stable coordination to Ag^+ ions occurs *via* the primary amino group, and low-temperature decomposition is promoted in the order of tertiary > secondary > primary amino groups of the distal position in a water-soluble family of alkyldiamines. We adopt *N*,*N*-dimethyl-1,3-propanediamine (dmpda) as one of the most promising candidates for realising an exclusive deposition method where water-soluble dmpda is a commercially available and inexpensive reagent. At the optimised reaction temperature of 70 °C, Ag NPs are completely deposited on TiO_2 particles within a few hours and the conversion efficiencies from Ag(I)–dmpda complexes into Ag NPs exceed 95%. The number-averaged particle sizes are increased from 6 to 15 nm, depending on the increased concentrations of Ag(I)–dmpda complexes with Ag weight ratios *versus* total weights of Ag and TiO_2 from 2 to 16 wt%. At this stage, the particle sizes are never controlled in the case of an Ag ratio of 16 wt% because the size distribution is becoming seriously wider as the concentrations of Ag(I)–dmpda complexes are increased. Nevertheless, the as-developed exclusive deposition method is of interest for advantageously preparing high-density Ag catalysts bearing immobilised nanosized Ag particles on the limited surface areas of TiO_2 particles. Our research is progressing toward our next reports that will clarify the crystal-growth mechanism of Ag NPs on TiO_2 particles and find the crucial factors for size-controllable and high-density deposition of Ag NPs on TiO_2 particles. It is noted that the water-based exclusive deposition method will be environmentally friendly, simple, low cost, and capable of the one-step and large-scale production of high-performance Ag NP catalysts on TiO_2 particles (Table 2), as well as saving expensive metal resources.

Conflicts of interest

There are no conflicts to declare.

Notes and references

1 J. E. van den Reijen, S. Kanungo, T. A. J. Welling, M. Versluijs-Helder, T. A. Nijhuis, K. P. de Jong and P. E. de Jongh, *J. Catal.*, 2017, **356**, 65–74.
2 A. Nagy and G. Mestl, *Appl. Catal., A*, 1999, **188**, 337–353.
3 K. Shimizu, Y. Miyamoto and A. Satsuma, *J. Catal.*, 2010, **270**, 86–94.
4 T. Mitsudome, M. Matoba, T. Mizugaki, K. Jitsukawa and K. Kaneda, *Chem.–Eur. J.*, 2013, **19**, 5255–5258.
5 T. Mitsudome, Y. Mikami, H. Funai, T. Mizugaki, K. Jitsukawa and K. Kaneda, *Angew. Chem., Int. Ed.*, 2008, **47**, 138–141.
6 H. Liu, D. Ma, R. A. Blackley, W. Zhou and X. Bao, *Chem. Commun.*, 2008, 2677–2679.
7 Z. Zhao, Y. Wang, J. Xu and Y. Wang, *RSC Adv.*, 2015, **5**, 59297–59305.
8 X.-Y. Dong, Z.-W. Gao, K.-F. Yang, W.-Q. Zhang and L.-W. Xu, *Catal. Sci. Technol.*, 2015, **5**, 2554–2574.
9 C. Wen, A. Yin and W.-L. Dai, *Appl. Catal., B*, 2014, **160–161**, 730–741.
10 P. Munnik, P. E. de Jongh and K. P. de Jong, *Chem. Rev.*, 2015, **115**, 6687–6718.
11 M. Okumura, T. Fujitani, J. Huang and T. Ishida, *ACS Catal.*, 2015, **5**, 4699–4707.
12 K. An and G. A. Somorjai, *ChemCatChem*, 2012, **4**, 1512–1524.
13 P. Claus and H. Hofmeister, *J. Phys. Chem. B*, 1999, **103**, 2766–2775.
14 N. Bogdanchikova, F. C. Meunier, M. Avalos-Borja, J. P. Breen and A. Pestryakov, *Appl. Catal., B*, 2002, **36**, 287–297.
15 J. Zhang, Y. Li, Y. Zhang, M. Chen, L. Wang, C. Zhang and H. He, *Sci. Rep.*, 2015, **5**, 12950.
16 A. Hernández-Gordillo, M. Arroyo, R. Zanella and V. Rodríguez-González, *J. Hazard. Mater.*, 2014, **268**, 84–91.
17 B. Xin, L. Jing, Z. Ren, B. Wang and H. Fu, *J. Phys. Chem. B*, 2005, **109**, 2805–2809.
18 S. Cai, H. Rong, X. Yu, X. Liu, D. Wang, W. He and Y. Li, *ACS Catal.*, 2013, **3**, 478–486.
19 S. C. Chen and M. A. Barteau, *Langmuir*, 2005, **21**, 5588–5595.
20 H. Zhang, G. Wang, D. Chen, X. Lv and J. Li, *Chem. Mater.*, 2008, **20**, 6543–6549.
21 N. Niño-Martínez, G. A. Martínez-Castañón, A. Aragón-Piña, F. Martínez-Gutierrez, J. R. Martínez-Mendoza and F. Ruiz, *Nanotechnology*, 2008, **19**, 065711.
22 X. You, F. Chen, J. Zhang and M. Anpo, *Catal. Lett.*, 2005, **102**, 247–250.
23 Q. Liu, Y. Cao, W.-L. Dai and J.-F. Deng, *Catal. Lett.*, 1998, **55**, 87–91.
24 B. Naik, V. S. Prasad and N. N. Ghosh, *Powder Technol.*, 2012, **232**, 1–6.
25 J. Ma, X. Guo, Y. Zhang and H. Ge, *Chem. Eng. J.*, 2014, **258**, 247–253.
26 C.-T. Dinh, T.-D. Nguyen, F. Kleitz and T.-O. Do, *ACS Appl. Mater. Interfaces*, 2011, **3**, 2228–2234.
27 Z.-J. Jiang, C.-Y. Liu and L.-W. Sun, *J. Phys. Chem. B*, 2005, **109**, 1730–1735.
28 Z. Jiang and C. Liu, *J. Phys. Chem. B*, 2003, **107**, 12411–12415.
29 M. Itoh, T. Kakuta, M. Nagaoka, Y. Koyama, M. Sakamoto, S. Kawasaki, N. Umeda and M. Kurihara, *J. Nanosci. Nanotechnol.*, 2009, **9**, 6655–6660.
30 T. Yamada, K. Fukuhara, K. Matsuoka, H. Minemawari, J. Tsutsumi, N. Fukuda, K. Aoshima, S. Arai, Y. Makita, H. Kubo, T. Enomoto, T. Togashi, M. Kurihara and T. Hasegawa, *Nat. Commun.*, 2016, **7**, 11402.
31 D. Wang, T. Xie, Q. Peng and Y. Li, *J. Am. Chem. Soc.*, 2008, **130**, 4016–4022.

32 M. Yamamoto, Y. Kashiwagi and M. Nakamoto, *Langmuir*, 2006, **22**, 8581–8586.
33 T. Togashi, K. Saito, Y. Matsuda, I. Sato, H. Kon, K. Uruma, M. Ishizaki, K. Kanaizuka, M. Sakamoto, N. Ohya and M. Kurihara, *J. Nanosci. Nanotechnol.*, 2014, **14**, 6022–6027.
34 H. K. Park, J. K. Yoon and K. Kim, *Langmuir*, 2006, **22**, 1626–1629.
35 K. Kim, H. S. Kim and H. K. Park, *Langmuir*, 2006, **22**, 8083–8088.
36 K. S. Shin, Y. K. Cho, J.-Y. Choi and K. Kim, *Appl. Catal., A*, 2012, **413–414**, 170–175.
37 T. Yahagi, T. Togashi, K. Kanaizuka and M. Kurihara, *Chem. Lett.*, 2016, **45**, 1195–1197.
38 P. Hervés, M. Pérez-Lorenzo, L. M. Liz-Marzán, J. Dzubiella, Y. Lu and M. Ballauff, *Chem. Soc. Rev.*, 2012, **41**, 5577–5587.
39 N. Pradhan, A. Pal and T. Pal, *Colloids Surf., A*, 2002, **196**, 247–257.
40 E. Menumerov, R. A. Hughes and S. Neretina, *Nano Lett.*, 2016, **16**, 7791–7797.
41 C. Kästner and A. F. Thünemann, *Langmuir*, 2016, **32**, 7383–7391.
42 L. R. S. Lara, A. D. Zottis, W. C. Elias, D. Faggion Jr, C. E. M. de Campos, J. J. S. Acuña and J. B. Domingos, *RSC Adv.*, 2015, **5**, 8289–8296.
43 W. Wu, M. Lei, S. Yang, L. Zhou, L. Liu, X. Xiao, C. Jiang and V. A. L. Roy, *J. Mater. Chem. A*, 2015, **3**, 3450–3455.
44 S. Tang, S. Vongehr and X. Meng, *J. Phys. Chem. C*, 2010, **114**, 977–982.
45 J. Qu, C. Ren, Y. Dong, Y. Chang, M. Zhou and X. Chen, *Chem. Eng. J.*, 2012, **211–212**, 412–420.
46 M. Wang, D. Tian, P. Tian and L. Yuan, *Appl. Surf. Sci.*, 2013, **283**, 389–395.
47 Y. Chi, Q. Yuan, Y. Li, J. Tu, L. Zhao, N. Li and X. Li, *J. Colloid Interface Sci.*, 2012, **383**, 96–102.
48 Z. Dong, X. Le, X. Li, W. Zhang, C. Dong and J. Ma, *Appl. Catal., B*, 2014, **158–159**, 129–135.
49 X. Wang, Z. Zhao, D. Ou, B. Tu, D. Cui, X. Wei and M. Cheng, *Appl. Surf. Sci.*, 2016, **385**, 445–452.